Proceedings of the XI DINAME, 28th February-4th March, 2005 - Ouro Preto - MG - Brazil
Edited by D.A. Rade and V. Steffen Jr.

MODAL VERSUS WAVE APPROACHES TO STRUCTURAL INTENSITY, FOR HIGHLY REVERBERANT STRUCTURES

Moyses Zindeluk
Federal University of Rio de Janeiro, UFRJ/COPPE/PEM
Cidade Universitária – Centro de Tecnologia – Bloco G, sala 204, Ilha do Fundão – Rio de Janeiro, RJ – 21945-970 - Brazil
moyses@serv.com.ufrj.br

Pedro Lisbôa Pereira Dias
Federal University of Rio de Janeiro, UFRJ/COPPE/PEM
Rua Senador Furtado, 109, casa 07 – Maracanã, Rio de Janeiro, RJ – 20270-021 - Brazil
pedrolpd@uol.com.br

Abstract. *Alternative approaches to the power flow evaluation in structures are discussed, the differences between the modal and wave techniques being stressed. Modal approaches, when real modes are used as a base, are reported to lead to some convergence slowness. This is mainly due to the fact that real modes are, in fact, standing waves, so the representation of the propagating fraction of the field would require complex modes to be used. Slow convergence would result from the implicit pseudo-modal character of the real mode representations. In the other hand, wave decomposition approaches, which should be considered as "exact", suffer from ill-conditioning, when applied to usual – highly reverberant – structures, since the energy flow sought is in fact a spillout of small differences among high amplitude components of mostly standing waves. Experimental results are shown, concerning a wave decomposition method for power flow in strongly reverberant mixed structures, e.g., structures that are commonly encountered in practical life. A comparison between wave decomposition method and a method which deals with correlations of measured accelerations, is presented. The main conclusions point to more accurate investigations about the behavior of such methods in structures "out of laboratory".*

Keywords: Wave, Power Flow, Energy, Modal, Damping.

1. Introduction

Since 1970, when Noiseux proposed the measurement of structural intensity for vibration analysis of structures, several papers have been published, dealing with formulations, methods and experimental results in structural components like beams and plates. Most of these works present results that are very "smooth", and very good agreement between theoretical and experimental results are presented. This happens mainly when the experimental specimens are true beams, plates, rods, bars, etc. But practical structures, structures that one can meet in real life, out of laboratory, are much more complex than those commonly used in laboratory, in spite of being combinations of simple structural elements: beams and plates, rods and beams, etc. These structures can be viewed as one-dimensional structures (beams) connected to two-dimensional structures (plates), for example, and are very reverberant, e.g., may present considerable modal density at low frequencies with small damping (Noiseux, 1970). A question that comes in mind is: how do the methods developed for intensity measurements work with these structures? Since experimental methods are very common in power flow studies, it is important to know how methods, developed and tested in laboratory, work in "real" structures.

The methods developed for practical intensity measurements can be classified as modal-based methods and wave-based methods. An example of modal-based method is the method of Pavic (1976) and Verheij (1980), and a wave-based method is the method of Halkyard and Mace (1995). Each of them has its advantages and disadvantages, and this paper aims to begin to establish limits of application of these methods to reverberant and complex structures, similar to those encountered in real life.

Several works report that very bad agreement between theoretical and experimental results is met when these methods are applied to reverberant structures (Piva, 2000; Dias, 2002), and also under other specific conditions (Bauman, 1994). The absence of damping in the theoretical predictions can explain, in part, as will be shown, this bad agreement.

Firstly, the present work shows a short review of the methods of Pavic (1976), Verheij (1980) and Halkyard and Mace (1995); secondly, a new equation for the intensity in Euler-Bernoulli beams with damping is shown; thirdly, experimental results are presented, in which intensity measurements were made in a very reverberant structure (Dias, 2002). Since structural intensity can be applied to the determination of energy transmission paths and energy sinks, aiding in redesign or structural modifications, conclusions are shown, which point to other ways of investigation of practical intensity measurements.

2. The Method of Pavic and Verheij

Verheij (1980) developed the Pavic (1976) method (which is, in fact, a correlation method, CM), in frequency domain. For an array of four accelerometers attached to an Euler-Bernoulli beam (Fig. 1), the final expression is:

$$\overline{w}_x(x,t) = \frac{EI}{\Delta^3}.\left[4\frac{1}{2w^3}\Im\{\widetilde{a}_2^*\,\widetilde{a}_3\} - \frac{1}{2w^3}\Im\{\widetilde{a}_2^*\,\widetilde{a}_4\} - \frac{1}{2w^3}\Im\{\widetilde{a}_1^*\,\widetilde{a}_3\}\right] \tag{1}$$

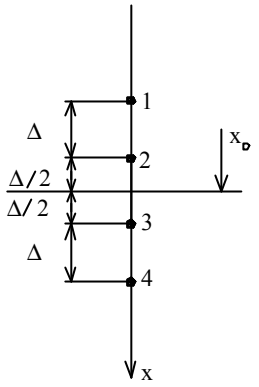

Figure 1. Array of four accelerometers attached to a beam.

in which $\overline{w}_x$ is the averaged intensity in the x direction, t is time, E is the elasticity modulus, I is the moment of inertia of area about centroidal axis, Δ is the distance between accelerometers, ω is the angular frequency, a is the acceleration signal, taken at the indicated position (1, 2, 3 or 4). An * means complex conjugate, while ~ means complex quantity. $\Im\{\bullet\}$ means imaginary part of $\bullet$.

Notice that, in the following text, when reference is made to the smaller sensor span, it means calculations with signals from "2" and "3" (near-fields not considered); when reference is made to the greater sensor span, it means calculations with signals from "1" and "4" (near-fields not considered); and finally, calculations with signals from "1", "2", "3" and "4" consider near-fields.

3. The Method of Halkyard and Mace

Halkyard and Mace (1995) developed a wave decomposition method (WDM). The final expression is:

$$\overline{w}_x(x,t) = EIwk^3\left[\left|\widetilde{A}\right|^2 - \left|\widetilde{B}\right|^2 + 2\left|\widetilde{C}\right|\left|\widetilde{D}\right|\mathrm{sen}(f)\right] \tag{2}$$

in which k is the flexural wavenumber, $\tilde{A}$ is the complex amplitude of the propagating wave in the positive direction, $\widetilde{B}$ is that for the propagating wave in the negative direction, $\widetilde{C}$ and $\widetilde{D}$ are the complex amplitudes of near-fields. ϕ is the phase angle between the complex amplitudes $\widetilde{C}$ and $\widetilde{D}$.

The complex amplitudes are calculated through:

$$\Phi = F^{-1}u \tag{3}$$

or

$$\Phi = (F^H F)^{-1}F^H u \tag{4}$$

in which:

$$\Phi = \begin{Bmatrix}\widetilde{A}\\ \widetilde{B}\\ \widetilde{C}\\ \widetilde{D}\end{Bmatrix} \qquad F = \begin{bmatrix} e^{-ikx_1} & e^{ikx_1} & e^{-kx_1} & e^{kx_1}\\ e^{-ikx_2} & e^{ikx_2} & e^{-kx_2} & e^{kx_2}\\ \vdots & \vdots & \vdots & \vdots\\ e^{-ikx_n} & e^{ikx_n} & e^{-kx_n} & e^{kx_n}\end{bmatrix} \qquad u = \begin{Bmatrix}u(x_1)\\ u(x_2)\\ \vdots\\ u(x_n)\end{Bmatrix} \tag{5}$$

n being the number of measurement points. For determined cases, if only two accelerometers (two measurements) are used, $\widetilde{A}$ and $\widetilde{B}$ are calculated, near-fields are not considered, and a 2x2 reduced form of (5) is used; if four

accelerometers (four measurement points) are used, $\widetilde{A}$, $\widetilde{B}$, $\widetilde{C}$ and $\widetilde{D}$ can be calculated, and near-fields are considered. In both cases, matrix F is square, and either Eq. (3) or (4) can be used. For overdetermined cases, if more than four measurement points are available, matrix F is not square, and Eq. (4) must be used.

4. Intensity with Damping

The methods described in sections **2** and **3**, as one can observe, do not take into account the effects of damping. Damping is responsible by the introduction of a phase profile change in the spatial-temporal movement of the dynamical system. For the development of Eq. (2), damping also was not taken into account, and various contributions to intensity consequently were not considered in the final formulation and, obviously, in the final calculations.

The version of Eq. (2) with damping being considered, is:

$$
\begin{aligned}
&\overline{w}_x(x,t)=\frac{1}{2}\cos(\eta)E_r I.\\
&\Big\{\omega k^3 e^{-2kx\sin\left(\frac{\eta}{4}\right)}\left|\widetilde{A}\right|^2\left[\cos(\alpha_1-\alpha_2)+\cos(\alpha_3-\alpha_4)\right]-\omega k^3 e^{2kx\sin\left(\frac{\eta}{4}\right)}\left|\widetilde{B}\right|^2\left[\cos(\beta_1-\beta_2)+\cos(\beta_3-\beta_4)\right]+\\
&+\omega k^3\left|\widetilde{A}\right\|\widetilde{B}\left|\left[\cos(\alpha_1+\beta_2)-\cos(\alpha_2+\beta_1)-\cos(\alpha_4+\beta_3)+\cos(\alpha_3+\beta_4)\right]+\right.\\
&+\omega k^3 e^{-kx\left[\cos\left(\frac{\eta}{4}\right)+\sin\left(\frac{\eta}{4}\right)\right]}\left|\widetilde{A}\right\|\widetilde{C}\left|\left[\cos(\alpha_1+\chi_2)-\sin(\alpha_2+\chi_1)+\sin(\alpha_4+\chi_3)-\cos(\alpha_3+\chi_4)\right]+\right.\\
&+\omega k^3 e^{kx\left[\cos\left(\frac{\eta}{4}\right)-\sin\left(\frac{\eta}{4}\right)\right]}\left|\widetilde{A}\right\|\widetilde{D}\left|\left[\cos(\alpha_1+\delta_2)+\sin(\alpha_2+\delta_1)-\sin(\alpha_4+\delta_3)-\cos(\alpha_3+\delta_4)\right]-\right.\\
&-\omega k^3 e^{-kx\left[\cos\left(\frac{\eta}{4}\right)-\sin\left(\frac{\eta}{4}\right)\right]}\left|\widetilde{B}\right\|\widetilde{C}\left|\left[\cos(\beta_1-\chi_2)-\sin(\beta_2-\chi_1)-\sin(\chi_3-\beta_4)-\cos(\beta_3-\chi_4)\right]-\right.\\
&-\omega k^3 e^{kx\left[\cos\left(\frac{\eta}{4}\right)+\sin\left(\frac{\eta}{4}\right)\right]}\left|\widetilde{B}\right\|\widetilde{D}\left|\left[\cos(\beta_1-\delta_2)+\sin(\beta_2-\delta_1)+\sin(\delta_3-\beta_4)-\cos(\beta_3-\delta_4)\right]+\right.\\
&+\omega k^3\left|\widetilde{C}\right\|\widetilde{D}\left|\left[\sin(\delta_2-\chi_1)-\sin(\chi_2-\delta_1)+\sin(\delta_3-\chi_4)-\sin(\chi_3-\delta_4)\right]+\right.\\
&\left.+\omega k^3\left(e^{-2kx\cos\left(\frac{\eta}{4}\right)}\left|\widetilde{C}\right|^2\left[\sin(\chi_2-\chi_1)-\sin(\chi_3-\chi_4)\right]-e^{2kx\cos\left(\frac{\eta}{4}\right)}\left|\widetilde{D}\right|^2\left[\sin(\delta_2-\delta_1)-\sin(\delta_3-\delta_4)\right]\right)\right\}
\end{aligned}
\tag{6}
$$

in which η is the loss factor (Cremer, Heckl and Ungar, 1988) of the material of the beam, E_r is the real part of the complex elasticity modulus of the material of the beam, and the phase angles a, b, c and d are calculated with the following expressions, in which ϕ_a, ϕ_b, ϕ_c and ϕ_d are the phase angles of the complex amplitudes $\widetilde{A}$, $\widetilde{B}$, $\widetilde{C}$ and $\widetilde{D}$, respectively:

$$
\begin{aligned}
\alpha_1&=\frac{3\eta}{4}+kx\cos\left(\frac{\eta}{4}\right)+\phi_a & \beta_1&=\frac{-3\eta}{4}+kx\cos\left(\frac{\eta}{4}\right)+\phi_b\\
\alpha_2&=\quad kx\cos\left(\frac{\eta}{4}\right)+\phi_a & \beta_2&=\quad kx\cos\left(\frac{\eta}{4}\right)+\phi_b\\
\alpha_3&=\frac{\eta}{4}+kx\cos\left(\frac{\eta}{4}\right)+\phi_a & \beta_3&=\frac{-\eta}{4}+kx\cos\left(\frac{\eta}{4}\right)+\phi_b\\
\alpha_4&=\frac{\eta}{2}+kx\cos\left(\frac{\eta}{4}\right)+\phi_a & \beta_4&=\frac{-\eta}{2}+kx\cos\left(\frac{\eta}{4}\right)+\phi_b
\end{aligned}
\tag{7}
$$

$$
\begin{aligned}
\chi_1&=\frac{-3\eta}{4}+kx\sin\left(\frac{\eta}{4}\right)-\phi_c & \delta_1&=\frac{-3\eta}{4}-kx\sin\left(\frac{\eta}{4}\right)+\phi_d\\
\chi_2&=\quad kx\sin\left(\frac{\eta}{4}\right)-\phi_c & \delta_2&=\quad -kx\sin\left(\frac{\eta}{4}\right)+\phi_d\\
\chi_3&=\frac{-\eta}{4}+kx\sin\left(\frac{\eta}{4}\right)-\phi_c & \delta_3&=\frac{-\eta}{4}-kx\sin\left(\frac{\eta}{4}\right)+\phi_d\\
\chi_4&=\frac{-\eta}{2}+kx\sin\left(\frac{\eta}{4}\right)-\phi_c & \delta_4&=\frac{-\eta}{2}-kx\sin\left(\frac{\eta}{4}\right)+\phi_d
\end{aligned}
\tag{8}
$$

Comparing Eq. (2) and Eq. (6), one can easily see that many contributions to intensity become part of the calculations by merely introducing damping in the form of the well-known loss factor of the material of the considered Euler-Bernoulli beam. The phase introduced by the loss factor make appear the contributions of the interaction between the propagating waves, the interaction between propagating waves and near-fields, and the near-fields among them.

5. Summary for the behavior of modal methods

The expected behavior of (real) modal representations for arbitrary motions of the system, in what concerns to the energy flow between the different degrees of freedom ("dof"), should be as outlined below (Zindeluk and Dias, 2004):

- For undamped systems, a consistent (non-zero average) "interdof" energy flow exists only when in transient vibration. A non-resonant steady state vibration, of harmonic or periodic nature, may be sustained by a driving force distribution, with zero net power flow, where "net" means averaged over an integer number of vibration periods. Still for undamped systems, free vibrations are conservative, each degree of freedom will carry constant mean energy, so mean energy flow is also null;

- For proportionally damped systems, still accurately representable through real modes, each dof will dissipate energy proportional to its energy level. Mean interdof energy flow is not needed for free (decaying) vibrations, but for unsteady and even for steady (harmonic or periodic) forced vibrations, energy flow should be representable, from the source(s) to the distributed sinks. Proportionally damped models are typical for structures, where modal damping factors are directly used to represent viscous or hysteretic distributed dissipation phenomena.

- The most interesting cases of application for structural intensity techniques are, however, the non-proportionally damped structures. This characteristic appears always when modeling a structure where damping devices or materials are applied to a portion of the structure, or particularly to part of the boundary. In this case, phase distortions due to damping will significantly deviate the structural response from the real modal representation. Hence, complex modes should be used for the most interesting cases, like the one dealt with, using different approaches, in this work.

6. Experiment Description

The experiment used a steel tank (1.400mm x 600mm x 600mm) supported by four wood pieces. One of the smaller sides of the tank was an aluminum plate, to the free edge of which an aluminum vertical beam was attached, with dimensions: length l = 1.800 mm, width b = 50.4 mm, thickness h = 2 mm. The mass density $\rho = 2.7 \times 10^3$ kg/m^3 and the elastic modulus $E = 7.1 \times 10^{10}$ Pa. The other (top) beam's edge was attached to the building through a natural rubber piece (absorbing edge), or a brass screw (reflecting edge). Excitation was provided by Brüel & Kjær 4810 mini-shaker, fixed at p = 15 cm below the top edge.

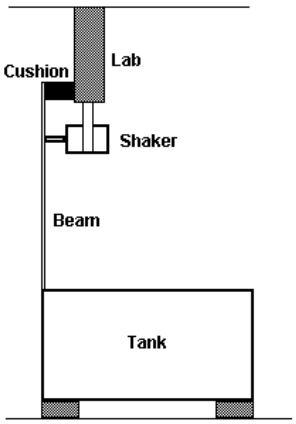

Figure 2. Schematic view of the experiment.

Other features of the experimental setup are:
- HP35665A spectrum analyzer; stationary white noise excitation (provided by HP analyzer source);
- shear accelerometers PCB 353M197 ICP; impedance head Brüel & Kjær 8001;
- Brüel & Kjær 2511 amplifier (for the impedance head); Brüel & Kjær 2706 amplifier (for the shaker);
- accelerometer arrays positioned at mid distance between excitation point and beam attachment to the tank (Fig. 3);
- accelerometers attached with bee wax;
- analyzer vector averaging function (10 samples);
- analyzer flattop window (for white noise excitation and good resolution for amplitude calculations);
- displayed analyzer resolution: 800 lines; span: 200 Hz; frequency resolution: 0.25 Hz; sampling time: 4s;
- accelerometers and the force sensor were relatively calibrated with the same shaker, frequency span and number of resolution lines. This relative calibration was done to obtain the phase difference spectrum between these sensors, in order to compensate it in the calculation of the average mechanical power injected to the structure;

– force spectrum was corrected due to the mass quantity (previously measured) that was between the impedance head and the structure (Ewins, 1984):

$$\begin{aligned} \Re\{F_{ap}\} &= \Re\{F_m\} - m\Re\{a\} \\ \Im\{F_{ap}\} &= \Im\{F_m\} - m\Im\{a\} \end{aligned} \tag{9}$$

in which F_{ap} is the applied force, F_m is the measured force, m is the mass located between impedance head force sensor and the structure, and $\Re\{\bullet\}$ is the real part of $\bullet$. Beam response measurements were done from 0 Hz to 400 Hz, in two bands: 0 Hz to 200 Hz, and 200 Hz to 400 Hz. Accelerometer was attached in distances that are ¼ of the wavelength of 100 Hz (central frequency of the band 0 Hz-200 Hz), and ¼ of the wavelength of 300 Hz (central frequency of the band 200 Hz-400 Hz). This ideal spacing Δ_f, for the frequency f, is calculated by:

$$\Delta_f = \frac{1}{4}\frac{2p}{k} = \frac{1}{4}\frac{2p}{\left[\frac{(2pf)^2 rS}{EI}\right]^{1/4}} \tag{10}$$

where S is beam cross section area, resulting in Δ_{100} = 10,78 cm and Δ_{300} = 6,23 cm. These distances are shown in Fig. 3, where right flags indicate spacing Δ_{100}, and left flags spacing Δ_{300}.

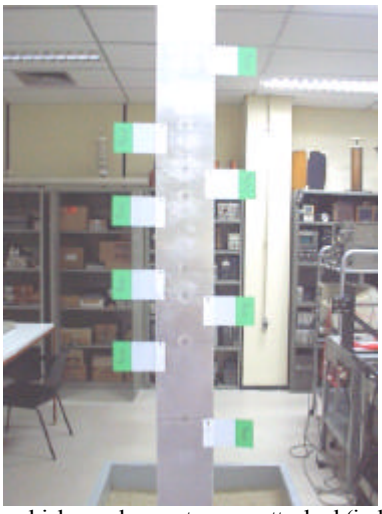

Figure 3. Positions where which accelerometer was attached (indicated by the paper flags)

The procedure for the experiment was:
– for each of the two upper boundary conditions, measurements were done in the distances shown in Fig. 3;
– measurement of the force applied to the structure;
– measurement of the acceleration imposed to the structure (in the same place where the force was measured).

7. Experimental Results

At low frequencies, the relatively long wavelengths of the waves that flow in the structure worsen the matrix conditioning. Due to this, calculated active averaged mechanical power cannot be close to the injected active averaged power. One may note a certain superiority of the correlation method over the wave decomposition method (Fig. 4).

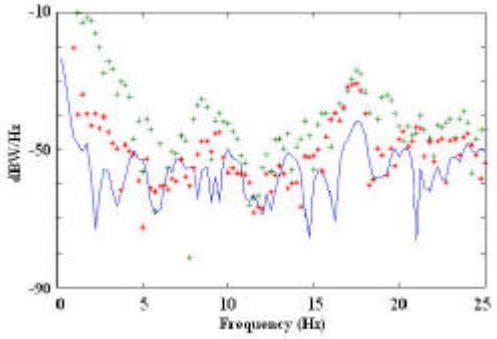

Figure 4. – injected active averaged mechanical power; + calculated active averaged mechanical power (WDM, near-fields considered); * calculated active averaged mechanical power (CM).

At relatively high frequencies (where many modes contribute to energy transfer), and with reflecting edge, all methods (WDM and CM) become closer (Fig. 5, Fig. 6 and Fig. 7). On the other hand, with the absorbing edge all methods tend to spread (Fig. 8, Fig. 9 and Fig. 10).

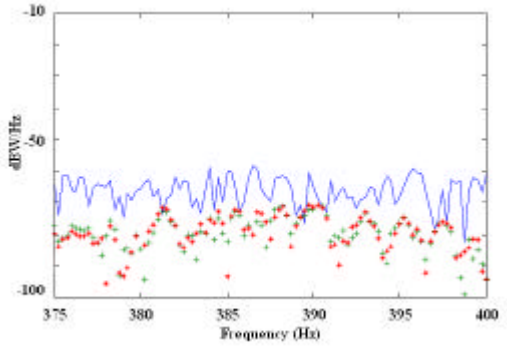

Figure 5. – injected active averaged mechanical power; + calculated active averaged mechanical power (WDM, near-fields considered); * calculated active averaged mechanical power (CM).

Hence, at relatively high frequencies, the difference between the edges (rubber piece and brass screw) is clearer. In the case of a reflecting edge WDM and CM cannot approach well the injected active averaged mechanical power (Fig. 11 and Fig. 12).

The conditioning of matrix F is a problem that affects WDM. Figure 13 shows theoretical condition numbers for matrix F. One can see that better conditioning is achieved in the middle frequencies of the two analyzed bands: 100 Hz (for 0 Hz to 200 Hz band) and 300 Hz (for 200 Hz to 400 Hz band).

On the other hand, Fig. 13(c) shows another theoretical condition number for matrix F. One can see that there are two frequencies in which the theoretical condition number is very bad. These frequencies are, respectively, 44.5 Hz and 177.75 Hz. The correspondent wavelengths are (Cremer and Heckl, 1988):

$$\frac{2\pi}{k} = \frac{2\pi}{\left[\frac{(2\pi 44{,}5)^2 \rho S}{EI}\right]^{1/4}} \cong 64{,}66\,\text{cm} \cong 6\Delta_{100} \cong 64{,}70\,\text{cm} \tag{11}$$

$$\frac{2\pi}{k} = \frac{2\pi}{\left[\frac{(2\pi 177{,}75)^2 \rho S}{EI}\right]^{1/4}} \cong 32{,}35\,\text{cm} \cong 3\Delta_{100} \cong 32{,}35\,\text{cm} \tag{12}$$

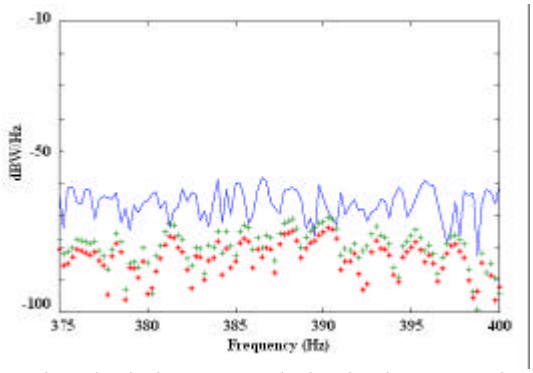

Figure 6. – injected active averaged mechanical power; + calculated active averaged mechanical power (WDM, near-fields considered); * calculated active averaged mechanical power (WDM, near-fields not considered; smaller sensor spacing considered).

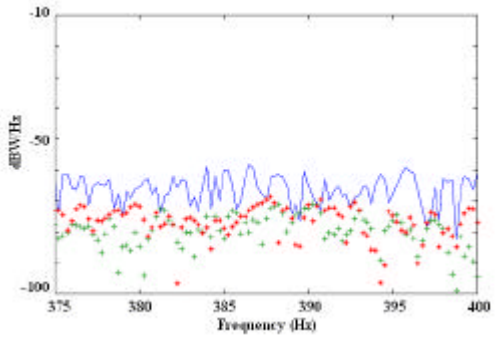

Figure 7. – injected active averaged mechanical power; + calculated active averaged mechanical power (WDM, near-fields considered); * calculated active averaged mechanical power (WDM, near-fields not considered; greater sensor spacing considered).

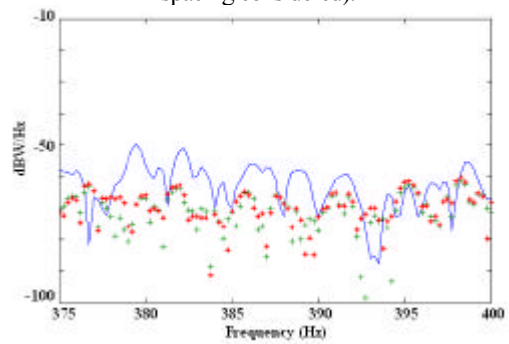

Figure 8. – injected active averaged mechanical power; + calculated active averaged mechanical power (WDM, near-fields considered); * calculated active averaged mechanical power (CM).

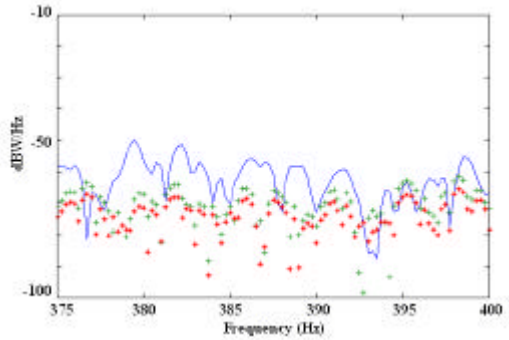

Figure 9. – injected active averaged mechanical power; + calculated active averaged mechanical power (WDM, near-fields considered); * calculated active averaged mechanical power (WDM, near-fields not considered, smaller sensors spacing considered).

For 44.5 Hz, the distance between accelerometer 1 and accelerometer 4 (Fig. 1) is half wavelength, and for 177.75 Hz (≅ 4 x 44.5Hz), distance between these accelerometers is one wavelength. It is clear how this bad conditioning affects calculation of the active averaged mechanical power by WDM: in Fig. 14, Fig. 15, Fig. 16 and Fig. 17, the arrow shows that bad conditioning makes the calculation to overestimate the calculated values in these frequencies.

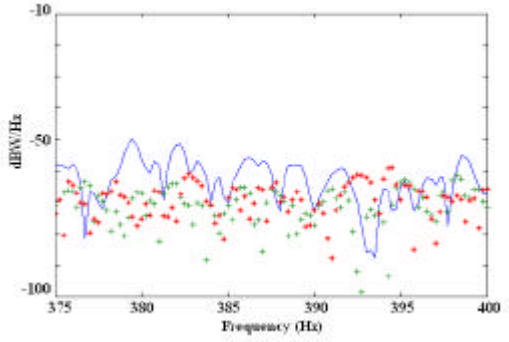

Figure 10. – injected active averaged mechanical power; + calculated active averaged mechanical power (WDM, near-fields considered); * calculated active averaged mechanical power (WDM, near-fields not considered, greater sensors spacing considered).

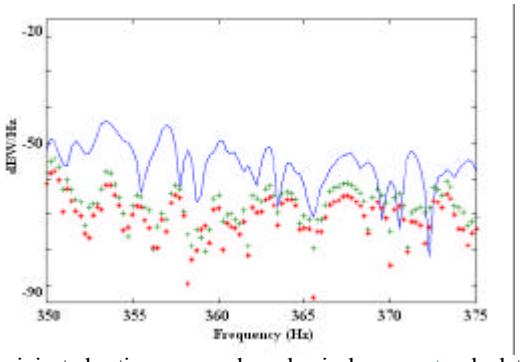

Figure 11. With rubber piece: – injected active averaged mechanical power; + calculated active averaged mechanical power (WDM, near-fields considered); * calculated active averaged mechanical power (CM).

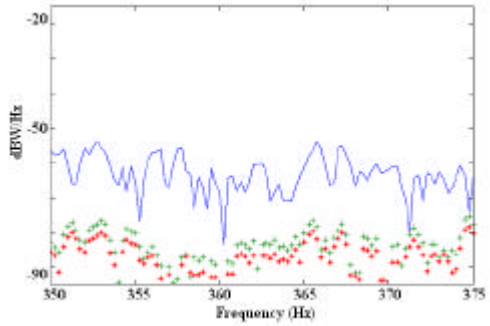

Figure 12. With brass screw: – injected active averaged mechanical power; + calculated active averaged mechanical power (WDM, near-fields considered); * calculated active averaged mechanical power (CM).

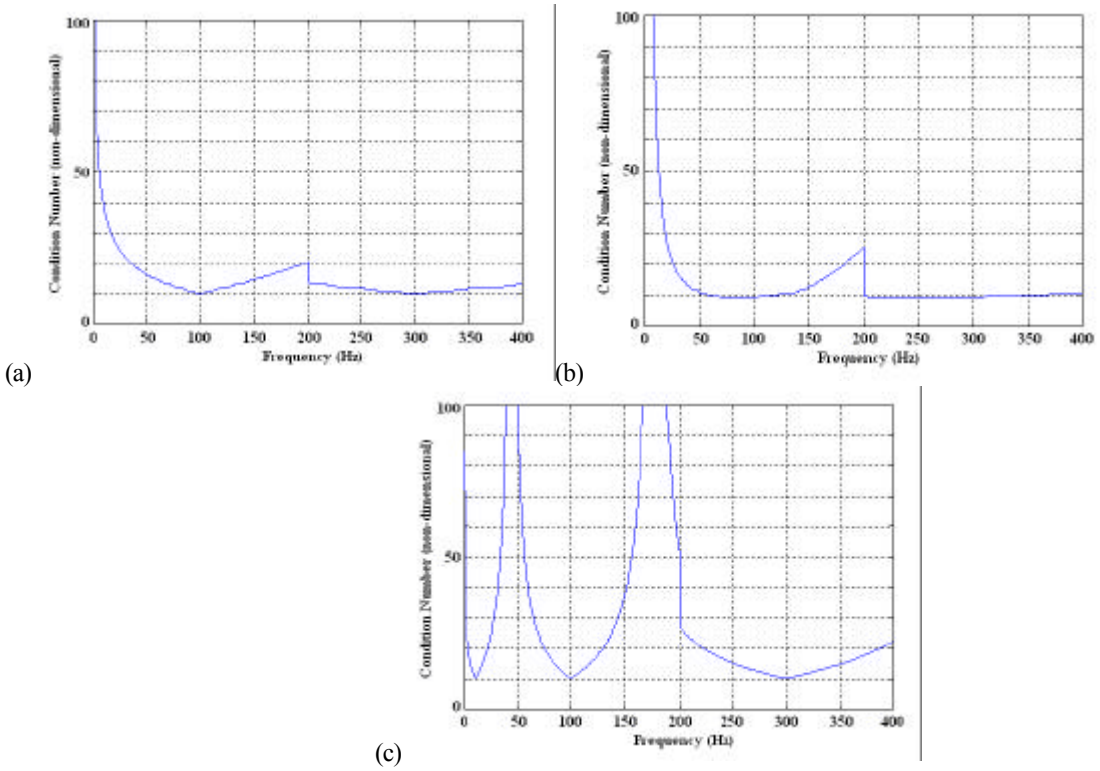

Figure 13. Theoretical condition number for matrix *F*. (a) near-fields not considered, smaller sensors spacing considered; (b) near-fields considered; (c) near-fields not considered; greater sensors span considered.

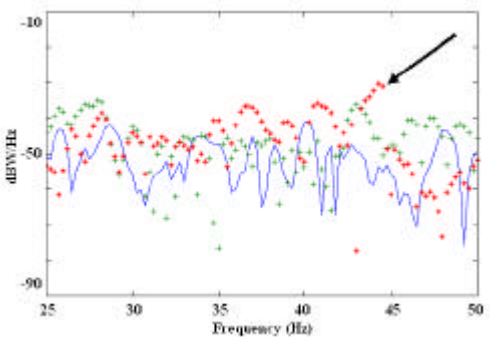

Figure 14. – injected active averaged mechanical power; + calculated active averaged mechanical power (WDM, near-fields considered); * calculated active averaged mechanical power (WDM, near-fields not considered, greater sensors span). With rubber piece (absorbing edge) used.

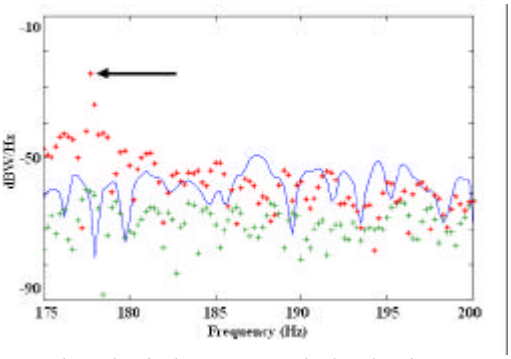

Figure 15. – injected active averaged mechanical power; + calculated active averaged mechanical power (WDM, near-fields considered); * calculated active averaged mechanical power (WDM, near-fields not considered, greater sensors spacing). With rubber piece (absorbing edge) used.

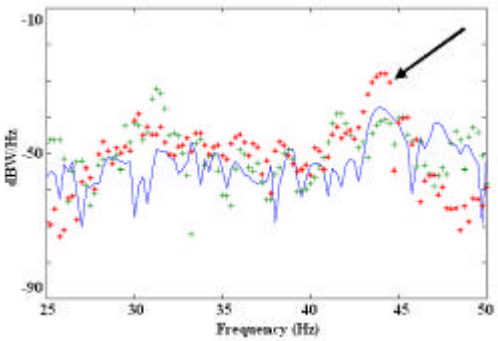

Figure 16. – injected active averaged mechanical power; + calculated active averaged mechanical power (WDM, near-fields considered); * calculated active averaged mechanical power (WDM, near-fields not considered, greater sensors span). With brass screw (reflected edge) used.

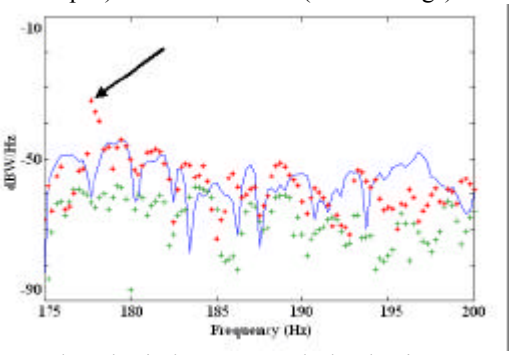

Figure 17. – injected active averaged mechanical power; + calculated active averaged mechanical power (WDM, near-fields considered); * calculated active averaged mechanical power (WDM, near-fields not considered, greater sensors spacing). With brass screw (reflected edge) used.

8. Concluding Remarks

With respect to the aspects tackled in this paper, the following was observed:

WDM, with near-fields not considered and greater sensors spacing, and CM, were the methods that gave best results in relatively low frequencies. This seems to be a strange result, since in lower frequencies the contributions of the near-fields should be important. However, it points to the need for more accurate calculations of the contributions of the near-fields, as shown in Eq. (6), and phase match between the sensors used. Unfortunately, Eq. (6) had not been developed when the experiments were done. It is expected that the use of Eq. (6) will give better results, since contributions of interactions of near-fields with propagating waves, and the contributions of near-fields themselves will be taken into account.

At relatively high frequencies, WDM approaches better the average injected active mechanical power. This is an expected result, since at high frequencies the contributions of the near-fields tend to disappear, and the non-accurate calculations of these contributions and phase mismatch of the sensors can be neglected.

When, for certain frequencies, sensor distances generate bad conditioning, CM is better to use than WDM, unless one uses sensor spacings that avoid bad conditioning at the frequencies of interest for the particular study. This shows a limitation to the use of WDM. However, Halkyard and Mace (1995) showed that there are other ways to overcome the ill-conditioning problem of the matrix of exponential terms in the frequencies of interest. The use of hybrid sensor arrays (accelerometers plus strain-gauges, for example), or the inclusion of an extra point of measurement, with the Moore-Penrose Generalized Inverse, as shown in Eq. (4), can improve WDM's results. This improvement in observability is similar to the one in controllability shown, for example, by Carvalho and Zindeluk (1999).

It is important, no matter the method used, to observe its behavior in practical situations, and to establish limits and conditions of application for intensity measurements with a specific method.

9. References

Bauman, P. D., 1994, "Measurement of Structural Intensity: Analytic and Experimental Evaluation of Various Techniques for the Case of Flexural Waves in One-Dimensional Structures", Journal of Sound and Vibration, Vol.174, No. 5, pp. 677-694.

Carvalho, M. O. M., Zindeluk, M., 1999, "Active Control of Waves on a Timoshenko Beam", PACAM VI: 6th PanamericanCongress of Applied Mechanics, DINAME 99: 8th International Conference on Dynamic Problems inMechanics, Rio de Janeiro.

Cremer, L., Heckl, M. and Ungar, E. E., 1988, Structure-Borne Sound, Structural Vibrations and Sound Radiation at Audio Frequencies. 2 ed., Springer-Verlag, Berlin.

Dias, P. L. P., 2002, Vibratory Energy Flow In Beams And Plates - Intensimetric Study. M.Sc. thesis, COPPE/UFRJ, Rio de Janeiro, RJ, Brazil (in portuguese).

Ewins, D. J., 1984, "Modal Testing: Theory and Practice", Research Studies Press Ltd. and John Wiley & Sons Inc., Great Britain, 269 p.

Halkyard, C. R. and Mace, B. R., 1995, "Structural Intensity in Beams – Waves, Transducer Systems and the Conditioning Problem", Journal of Sound and Vibration, Vol.185, No. 2., pp. 279-298.

Noiseux, D. U., 1970, "Measurement of Power Flow in Uniform Beams and Plates", Journal of The Acoustical Society of America, Vol.47, No. 1, pp. 238-247.

Pavic, G., 1976, "Measurement of Structure Borne Wave Intensity, Part I: Formulation of the Methods", Journal of Sound and Vibration, Vol.49, No. 2, pp. 221-230.

Piva, J. I., 2000, Experimental Determination of Power Flow in Beams. M.Sc. thesis, Faculdade de Engenharia Mecânica da Universidade Estadual de Campinas, Campinas, SP, Brazil, 2000 (in portuguese).

Verheij, J. W., 1980, "Cross Spectral Density Methods for Measuring Structure Borne Power Flow on Beams and Pipes", Journal of Sound and Vibration, Vol.70, No. 1, pp. 133-139.

Zindeluk, M., and Dias, P. L. P., 2004, "Wave Propagation and Modal Approaches to Structural Power Flow", Proceedings of the 33rd International Congress on Noise Control Engineering, Inter-Noise 2004, Prague, Czech Republic.